Experimental and theoretical investigation of the impact of ultra-fast carrier dynamics on high-speed SOA-based all-optical switches

Mads L. Nielsen and Jesper Mørk

Research Center COM, Technical University of Denmark, Bldg. 345v, DK-2800 Kgs. Lyngby, Denmark
jm@com.dtu.dk

Rei Suzuki, Jun Sakaguchi, and Yoshiyasu Ueno

Graduate School of Electronic Engineering, University of Electro-Communications, 1-5-1 Chofugaoka, Chofu, Tokyo, 182-8585, Japan

Abstract: The impact of ultra-fast carrier dynamics in semiconductor optical amplifiers (SOAs) on switches based on cross-gain and cross-phase modulation is analyzed theoretically and experimentally. We find that ultra-fast effects lead to additional spectral broadening, which improves the optical signal-to-noise ratio for switches based on an SOA and an optical filter. For such switches, the influence of ultra-fast effects on the so-called nonlinear patterning effect is analyzed for three filter configurations: the asymmetric Mach-Zehnder interferometer (AMZI), a band-pass filter (BPF), and a cascade of an AMZI and a BPF. We conclude that fast carrier dynamics dramatically reduces nonlinear patterning and that the successful high-speed (>100 Gb/s) demonstrations in the literature rely on these effects.

©2006 Optical Society of America

OCIS codes: (060.2330) Fiber optics communications; (250.5980) Semiconductor optical amplifiers

References and links

1. H. J. S. Dorren, M. T. Hill, Y. Liu, E. Tangdiongga, M. K. Smit, and G. D. Khoe, "Optical signal processing and telecommunication applications," in OAA Topical Meeting 2005 on CD-ROM, WD1 (2005).
2. A. Mecozzi, and J. Mørk, "Saturation induced by picosecond pulses in semiconductor optical amplifiers," J. Opt. Soc. Am. B **14**, 761 (1997).
3. J. Mørk, T. W. Berg, M. L. Nielsen, and A. V. Uskov, "The role of fast carrier dynamics in SOA based devices," IEICE Trans. Electron. **E87-C**, 1126 (2004).
4. S. Nakamura, Y. Ueno, and K. Tajima, "Femtosecond switching with semiconductor-optical-amplifier-based symmetric Mach-Zehnder-type all-optical switch," Appl. Phys. Lett. **78**, 3929 (2001).
5. J. Mørk, and A. Mecozzi, "Theory of the ultrafast optical response of active semiconductor waveguides," J. Opt. Soc. Am. B **19**, 1803 (1996).
6. A. Mecozzi, and J. Mørk, "Saturation effects in non-degenerate four-wave mixing between short optical pulses in semiconductor laser amplifiers," IEEE J. Sel. Top. Quantum Electron. **3**, 1190 (1997).
7. A. K. Mishra, X. Yang, D. Lenstra, G.-D. Khoe, and H. J. S. Dorren, "Wavelength conversion employing 120 fs optical pulses in an SOA-based nonlinear polarization switch," IEEE J. Sel. Top. Quantum Electron. **10**, 1180 (2004).
8. M. L. Nielsen, and J. Mørk, "Increasing the modulation bandwidth of semiconductor optical amplifier based switches using optical filtering," J. Opt. Soc. Am. B. **21**, 1606 (2004).
9. Y. Ueno, S. Nakamura, H. Hatekeyama, T. Tamanuki, T. Sasaki, and K. Tajima, "168 Gb/s OTDM wavelength conversion using an SMZ-type all-optical switch," in *Proceedings of ECOC 2000,* Vol. **1**,(European Conference on Optical Communications, Munich, Germany, 2000) pp. 13-14.
10. J. Leuthold, B. Mikkelsen, G. Raybon, C. H. Joyner, J. L. Pleumeekers, B. I. Miller, K. Dreyer, and R. Behringer, "All-optical wavelength conversion between 10 and 100 Gb/s with SOA delayed-interference configuration," Opt. Quantum Electron. **33**, 939 (2001).

#8897 - $15.00 USD Received 26 September 2005; revised 22 November 2005; accepted 19 December 2005

11. Y. Liu, E. Tangdiongga, Z. Li, S. Zhang, H. de Waardt, G. D. Khoe, and H. J. S. Dorren, "160 Gb/s SOA-based wavelength converter assisted by an optical bandpass filter," Technical Digest of OFC 2005, **PDP 17**, Anaheim, CA. (2005).
12. M. L. Nielsen, B. Lavigne, and B. Dagens, "Polarity-preserving wavelength conversion at 40 Gb/s using band-pass filtering," IEE Electron. Lett. **39**, 1334 (2003).
13. Y. Liu, E. Tangdiongga, Z. Li, S. Zhang, H. de Waardt, G. D. Khoe, and H. J. S. Dorren, "80 Gb/s wavelength conversion using semiconductor optical amplifier and optical bandpass filter," IEE Electron. Lett. **41**, 487 (2005).
14. M. L. Nielsen, and J. Mørk, "Bandwidth enhancement of SOA-based switching using optical filtering: theory and experiment," in Proceedings of ECOC 2005, (European Conference on Optical Proceedings, Glasgow, UK 2005) paperTu3.5.7.
15. M. L. Nielsen, J. Mørk, J. Sakaguchi, R. Suzuki, and Y. Ueno, "Reduction of nonlinear patterning effects in SOA-based all-optical switches using optical filtering," Technical Digest of OFC 2005, (Anaheim, CA., 2005) paper OThE7.
16. Y. Ueno, S. Nakamura, and K. Tajima, "Nonlinear phase shifts induced by semiconductor optical amplifiers with control pulses at repetition frequencies in the 40-160 GHz range for use in ultrahigh-speed all-optical signal processing," J. Opt. Soc. Am. B **19**, 2573 (2002).
17. M. L. Nielsen, J. Mørk, R.Suzuki, J. Sakaguchi, and Y. Ueno," Theoretical and experimental study of fundamental differences in the noise suppression of high-speed SOA-based all-optical switches," Opt. Express **13,** 5080 (2005), http://www.opticsexpress.org/abstract.cfm?URI=OPEX-13-13-5080
18. M. L. Nielsen, "Experimental and theoretical investigation of semiconductor optical amplifier (SOA) based all-optical switches," Ph. D. thesis, Research Center COM, Technical University of Denmark (2004).
19. Y. Ueno, "Theoretically predicted nonlinear phase imbalance for delayed-interference signal-wavelength converters (DISC)," Jpn. J. Appl. Phys. **43**, L665 (2004).
20. J. Leuthold, D. M. Maron, S. Cabot, J. J. Jaques, R. Ryf, and C. R.Giles, "All-optical wavelength conversion using a pulse reformatting optical filter," J. Lightwave Technol.. **22**, 186 (2004).
21. G. P. Agrawal, N. and A. Olsson, "Self phase modulation and spectral broadening of optical pulses in semiconductor laser amplifiers," J. Quantum Electron. **25**, 2297 (1989).
22. P. Borri, S. Scaffetti, J. Mørk, W. Langbein, J. M. Hvam, A. Mecozzi, and F. Martelli, "Measurement and calculation of the critical pulsewidth for gain saturation in semiconductor optical amplifiers," Opt. Commun. **164**, 51 (1999).
23. A. D. Ellis, A. E. Kelly, D. Nesset, D. Pitcher, D. G. Moodie, and R. Kashyap, "Error-free 100 Gb/s wavelength conversion using grating assisted cross-gain modulation," Electron. Lett. **34**, 1958 (1998).
24. T. Akiyama, K. Kawaguchi, M. Ekawa, M. Sugawara, H. Kuwatsuka, H. Sudo, K. Otsubo, S. Okumura, A. Uetake, F. Futami, and S. Watanabe, "Recent progress in quantum-dot semiconductor optical amplifiers for optical signal processing," in OAA Topical Meeting 2005 on CD-ROM, MB1 (2005)

1. Introduction

As the need for capacity in optical transmission systems and networks increases, it may be feasible to operate wavelength division multiplexed (WDM) channels at bitrates exceeding the bandwidth of electronic drivers and optoelectronic modulators. In this scenario optical time-division multiplexing (OTDM) offers a solution by passively interleaving lower bitrate return-to-zero (RZ) channels consisting of very short pulses, into a single high-speed data stream. It is predicted that such systems will benefit from employing optical signal processing for relatively simple functionalities, such as wavelength conversion, regeneration, and very basic logic processing related to e.g. performance monitoring. The building block in optical signal processors is the optical switch or gate, which has been demonstrated at bitrates exceeding 100 Gb/s using nonlinearities in Silica fibers, periodically-poled $LiNbO_3$ crystals, and semiconductor optical amplifiers (SOAs). SOA-based solutions possess a number of attractive features such as low power consumption, small footprint and relatively high bandwidth, which makes them the current technology-of-choice [1].

When the data bitrate increases, the width of the data pulses must decrease. Signal processing in SOAs is based on saturation of the gain and refractive index, and the nature of the saturation process changes qualitatively when the pulse width drops below a certain critical limit [2]. This originates from the existence of ultra-fast intra-band carrier dynamic processes, due primarily to spectral hole-burning (SHB) and carrier heating (CH) [1-7], which are effective on time scales on the order of 1 ps or less. Ultra-fast carrier dynamics in SOAs and lasers has been studied extensively [1-7], and accurate mathematical models have been developed [2, 5-7]. Most published investigations of ultra-fast phenomena focus on the gain

#8897 - $15.00 USD Received 26 September 2005; revised 22 November 2005; accepted 19 December 2005
(C) 2006 OSA

and phase response to a single short pulse or a periodic train of short pulses [2, 4-7], which reveals details that can be verified through pump-probe experiments. However, from a systems perspective it is crucial to understand how SOA-based devices are influenced by ultra-fast dynamics when subjected to a random *data* signal (which will also be denoted *control* signal in the paper), since non-periodic gain and phase modulation leads to patterning effects on the switched signal.

The patterning effect may be divided into two contributions, *linear* and *nonlinear patterning* (NLP), named after their dependence on the gain modulation in the carrier rate Eq. [8]. Linear patterning is due to the relatively slow carrier recovery, and can be compensated for by a passive filter, which equalizes the optical response [8]. By eliminating linear patterning, the width of the switching window is only limited by the control pulse width. However, the saturation of the gain leads to a nonlinear variation, i.e. nonlinear patterning, of the energy of the short, switched pulses, which cannot easily be suppressed. For a detailed discussion of linear versus nonlinear patterning, the reader is referred to Ref. [8].

In recent years, all-optical switches composed of an SOA followed by an optical filter have received considerable attention due to their simplicity and high-speed performance [1,3,8-20]. A generic configuration is illustrated in Fig. 1, where a control signal modulates the phase of a continuous wave (CW) beam at a different wavelength through the carrier dynamics, and a filter converts the phase modulation into amplitude modulation. After the filter, a linear amplifier boosts the signal power.

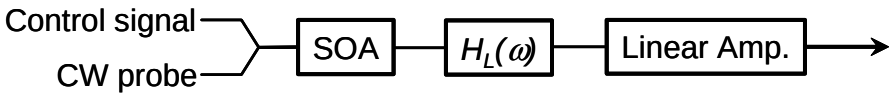

Fig. 1. Schematic of all-optical switch based on a single SOA and an optical filter. $H_L(\omega)$ is the filter's field transfer function.

Mainly two types of filters have been studied, namely the asymmetric Mach-Zehnder interferometer (AMZI) and a simple band-pass filter (BPF), detuned from the probe carrier frequency. The combination of an SOA and AMZI is commonly referred to as a delayed-interference signal converter (DISC) [9-11], and has demonstrated wavelength conversion at bitrates up to 168 Gb/s [9-11]. The AMZI has also been shown to completely compensate for linear patterning effects [8,14]. The simple SOA+ detuned BPF configuration has similar properties [8], and wavelength conversion at 40 Gb/s [12] and 80 Gb/s [13] has been demonstrated so far.

It has been suggested by Liu et al. [1,11] that the fast response of switches based on an SOA and a filter, allowing for high-speed, large-signal operation, can be ascribed to ultra-fast carrier dynamics. In this paper we investigate this in detail, theoretically as well as experimentally. The impact of ultra-fast carrier dynamics on the cross-phase modulation (XPM) induced broadening of the probe spectrum is studied, as well as the NLP induced by switches based on an SOA followed by a filter. We implement the model of Mecozzi and Mørk [2], using parameters extracted from measurements, and compare with results of experiments with high temporal resolution. We find that ultra-fast dynamics significantly impacts the optical spectrum of the switched signal, and verify an experimentally observed excessive broadening on the blue side of the probe carrier. Moreover, a previously published analytical relationship between the induced phase modulation and the suppression of the first harmonic in the power spectrum, derived without taking ultra-fast effects into account [16], is shown to be equally accurate in the presence of fast dynamics. An AMZI filter is realized experimentally in the polarization domain [9], and through comparison with simulations we experimentally verify the conclusion in Ref. [3] that the nonlinear gain suppression, caused by SHB and CH, reduces NLP at the DISC output. This aids in understanding why the DISC can operate successfully at bitrates exceeding 100 Gb/s. We reach the same conclusion for the

#8897 - $15.00 USD Received 26 September 2005; revised 22 November 2005; accepted 19 December 2005
(C) 2006 OSA

simple SOA+BPF switch, and generally observe very good correspondence between experimental waveforms and waveforms simulated with the model including ultra-fast effects.

Cascading the AMZI and the detuned BPF, we optimize the filter transfer function and obtain additional reduction of the nonlinear patterning. The advantage of cascading the AMZI and detuned BPF is consistent with the reports in Refs. [10, 11, 15].

The paper is organized as follows: section 2 briefly reviews the numerical model, accounts for the choice of parameters and presents a comparison between calculated and measured cross-gain modulation (XGM) traces. In section 3, the impact of ultra-fast dynamics on the relationship between the spectral components in the optical power spectrum of the probe is investigated for a periodic 42 GHz control signal. Finally, section 4 analyses the NLP of the switched probe signal for an SOA followed by an AMZI (the DISC switch), a detuned BPF, and a filter consisting of a cascade of an AMZI and a detuned BPF. Section 5 summarizes and concludes the paper.

2. Numerical model

In the following, the model of Mecozzi and Mørk [2] will be briefly reviewed. For a detailed description of the model and the underlying physics, the reader is referred to Refs. [2,5].

The model presented in Ref. [2] includes the nonlinear effects of carrier heating (CH) and spectral holeburning (SHB), and may be considered a generalization of the often-used linear model of Agrawal and Olsson [21]. Both models neglect the loss in the SOA waveguide, and assume that the carrier density dependent (linear) material gain $g_l(N) = a(N - N_{tr})$ is a linear function of the carrier density N, with a and N_{tr} being the differential gain and transparency carrier density, respectively. Furthermore, the influence of intra-band dynamics is modeled through a nonlinear gain suppression factor $\varepsilon = \varepsilon_{CH} + \varepsilon_{SHB}$ with contributions from both CH and SHB [2]. This approach assumes that the pulse width exceeds the intra-band carrier scattering time and the temperature relaxation time, which are on the order of 100 fs and 1 ps, respectively [5]. With this assumption the impact of CH and SHB can be considered instantaneous and the material gain can be expressed as $g = g_l(N)/(1+\varepsilon S)$, where S is the photon density. In this work a pulse width just below 2 ps is used and consequently the model is expected to be reasonably accurate; for shorter pulses the more general model of Ref. [6] may be applied.

We consider the case where a control signal of short pulses are launched into the SOA along with a strong saturating CW probe beam, acting as a holding beam reducing the effective carrier lifetime τ_e, which is the timescale on which the carrier density recovers when the contribution from stimulated recombination is taken into account. The spatial evolution of the photon density and the carrier density is described by [2]

$$\frac{dS_k}{dz} = \frac{\Gamma a(N - N_{tr})}{1+\varepsilon\left(S_{cntr} + S_{probe}\right)} S_k \tag{1}$$

$$\frac{dN}{dt} = \frac{I}{eV} - \frac{N}{\tau_{sp}} - \frac{v_g a(N - N_{tr})}{1+\varepsilon\left(S_{cntr} + S_{probe}\right)}\left(S_{cntr} + S_{probe}\right) \tag{2}$$

where k in Eq (1) represents either the control signal or the CW probe beam (k = "*cntr*" or "*probe*"), and Γ is the confinement factor. In Eq. (2) I, e, V, τ_{sp}, v_g, S_{cntr} and S_{probe} are the injection current, elementary charge, active waveguide volume, spontaneous carrier lifetime, group velocity, and photon densities associated with the control signal and CW probe, respectively. Equation (2) can be simplified further by noting that S_{cntr} is zero between pulses and that the contribution from S_{CW} to the nonlinear gain may be neglected during the pulses

#8897 - $15.00 USD Received 26 September 2005; revised 22 November 2005; accepted 19 December 2005
(C) 2006 OSA

$$\frac{dN}{dt} = -\frac{N - N_0}{\tau_e} - \frac{v_g a (N - N_{tr})}{1 + \varepsilon S_{cntr}} S_{cntr} \tag{3}$$

Here, N_0 is the steady state carrier density when the control signal is off. It is used that $\tau_e^{-1} = \tau_{sp}^{-1} + v_g a S_{CW}$, where $S_{CW} = S_{probe}(0)$, which is assumed constant although S_{CW} is time dependent through the gain. The approximation in Eq. (3) is also made in Ref. [2] by neglecting the gain saturation by the probe signal and choosing $\tau_{sp} = \tau_{eff}$. When fitting parameters to experimental data, Eq. (3) is more convenient than Eq. (2), as it breaks the relationship between the gain and the effective carrier lifetime. We are assuming that the probe and data signals are separated by less than the homogeneous linewidth (typically on the order of a few tens of nm) such that the gain can be taken equal for the data and the probe signal.

Introducing the unsaturated modal gain $g_{m,0}(z) = \Gamma a (N_0 - N_{tr}) z$ and the integrated saturated modal gain $g_m(t,z) = \ln G(t,z) = \ln\left(S(t,z)/S(t,0)\right)$, Eqs. (1) and (3) may be integrated to provide the following differential equation for the temporal and spatial dependence of $g_m(t,z)$ [2]

$$\begin{aligned} \frac{dg_m(t,z)}{dt} = & \frac{1}{1 + \varepsilon \exp\left[g_m(t,z)\right] S(t,0)} \\ & \times \left[-\left\{\exp\left[g_m(t,z)\right] - 1\right\} \left(v_g a + \varepsilon \frac{d}{dt} \right) S(t,0) - \frac{1}{\tau_e} \left[g_m(t,z) - g_{m,0}(z) \right] \right. \\ & \left. + \varepsilon \left\{\exp\left[g_m(t,z)\right] - 1\right\} S(t,0) \right] \end{aligned} \tag{4}$$

Here it should be noticed that by setting $\varepsilon = 0$, Eq. (4) is reduced to the result of Agrawal and Olsson [21]. The solution to Eq. (4) provides the gain $G(t,z) = \exp\left[g_m(t,z)\right]$, and thus the output probe power $S_{probe}(z,t) = G(t,z) S_{probe}(z=0)$. Analogously to the gain, the phase modulation has a linear and a nonlinear contribution. Of the two intra-band effects considered here, only CH contributes, since SHB does not add to the phase shift as long as the spectral hole is symmetric, which is the case if the wavelength of the pulsed signal is close to the gain peak of the SOA [2,5]

$$\begin{aligned} \Phi(t,z) &= \Phi_N(t,z) + \Phi_{CH}(t,z) \\ &= -\frac{1}{2} \alpha_N \left[g_{m,lin}(t,z) - g_{m,0}(z) \right] \\ &\quad + \frac{1}{2} \alpha_{CH} \varepsilon_{CH} \left\{\exp\left[g_m(t,z)\right] - 1\right\} S_{pulse}(t,0) \end{aligned} \tag{5}$$

Here, $\Phi_N(t,z)$ and $\Phi_{CH}(t,z)$ are the linear (carrier density dependent) and CH-induced contributions to the total phase shift $\Phi(t,z)$. α_N is the linewidth enhancement factor, i.e. the coupling between phase and amplitude, due to a carrier density change, and

#8897 - $15.00 USD Received 26 September 2005; revised 22 November 2005; accepted 19 December 2005
(C) 2006 OSA

$g_{m,lin}(t,z) = \ln G(t,z) + \varepsilon\left[G(t,z)-1\right]S_{pulse}(t,0)$ is the linear equivalent of $g_m(t,z)$, i.e., the integrated linear modal gain. The coupling between the phase change and the change of electron temperature is described by the parameter α_{CH}. The contribution to CH from the holes can be neglected, since the heavier mass leads to shorter temperature relaxation time, and hence lower gain suppression factor, than for the electrons [6].
From the solutions of eqs. (4-5) the electrical probe field, in units of $W^{½}$, at the SOA output can be expressed as

$$E_{probe}(t,L) = \sqrt{G(t,L)\xi S_{probe}(0)}\exp\left[j\phi(t,L)\right] \tag{6}$$

Here, L is the SOA length and $\xi = EAv_g/\Gamma$ is the conversion factor from photon density to optical power, with E and A being the photon energy and waveguide cross section area, respectively.

The action of the optical filter, described by a field transfer function $H_F(\omega)$, is conveniently described in the frequency domain

$$E_F(t) = F^{-1}\left\{H_F(\omega)F\left[E_{probe}(t,L)\right]\right\} \tag{7}$$

where $F[\cdot]$ and $F^{-1}[\cdot]$ are the Fourier transform and inverse Fourier transform, respectively. In Eq. (7), $H_F(\omega)$ should be substituted by the appropriate field transfer function for the AMZI [8] or the Gaussian BPF, used in section 4

$$H_{AMZ}(\omega) = ½\left[1+\exp\left[j\left(\omega\tau+\Phi_0\right)\right]\right] \tag{8}$$

$$H_{gauss}(\omega) = \exp\left[-2\ln(2)\left(\frac{\omega-\Delta\omega}{\Delta\omega_{3dB}}\right)^2\right] \tag{9}$$

In Eq. (8), τ and Φ_0 are the differential delay and phase bias of the AMZI filter, and in Eq. (9) $\Delta\omega$ is the detuning from the carrier angular frequency and $\Delta\omega_{3dB}$ is the full width at half maximum (FWHM) bandwidth.

In order to solve Eqs. (4-9) numerically the parameters $g_{m,0}$, a, Γ, A, τ_e, α_N, α_{CH}, ε_{SHB}, ε_{CH}, the FWHM width τ_p of the sech^2 control pulses, τ, and the input probe power $P_{CW} = P_{probe}(0)$ must be fixed, and the chosen values are given in Table 1 below. Details regarding the dimensions of the commercial SOA were not available, but since Γ depends on A, an effective index estimation of the confinement factor was carried out for a typical waveguide cross section. For the differential gain a and the α_{CH}-parameter, we chose values typically reported in the literature [2,5,22]. The choice of the α_N-parameter and the effective carrier lifetime τ_e, corresponding to the experimentally used input probe power level, were based on previous measurements on the same device [14], whereas the steady state chip gain

#8897 - $15.00 USD Received 26 September 2005; revised 22 November 2005; accepted 19 December 2005
(C) 2006 OSA

$G_0 = \exp\left[g_{0,m}(L)\right]$ was measured taking the SOA's coupling losses into account. The latter were carefully characterized as a function of the input power for different wavelengths. For the probe wavelength of 1558 nm used in the experiments, the coupling loss at the input facet was measured to 3.5 dB for an input power in the fiber of 6 dBm, which is the CW power used in all the measurements. The corresponding coupling loss at the output facet was 4 dB. Thus, a measured fiber-to-fiber gain of 5.5 dB corresponds to a chip gain of 13 dB. For the gain suppression factors, the value of ε_{SHB} was based on the references [2,5,22], while ε_{CH} was fitted to provide waveforms at the DISC output resembling the experimental results. In the experiments the output of the switch is cross correlated with 1.8 ps wide (FWHM) pulses, so before comparing the simulated pulse traces to the measured results they are convoluted with a 1.8 ps wide sech^2 pulse. Unless otherwise mentioned, the control pulse width is always 1.8 ps. It should be noted that the chosen value for ε_{CH} is within the range reported in the literature [22].

Table 1. Simulation parameters

Parameter	Value
Steady-state chip gain G_0 at 1558 nm (for $P_{probe}(0) = 2.5\ dBm$)	$13\,dB$
Differential gain a	$3.5 \cdot 10^{-20}\ m^2$
Optical confinement factor Γ	0.40
Waveguide cross section area A	$2.4 \cdot 10^{-13}\ m^2$
Effective carrier lifetime τ_e	$60\ ps$
α_N -parameter	7.0
α_{CH} -parameter	3.0
SHB gain suppression factor ε_{SHB}	$0.7 \cdot 10^{-23}\ m^3$
CH gain suppression factor ε_{CH}	$1.9 \cdot 10^{-23}\ m^3$
Sech^2 FWHM control signal pulse width	$1.8\ ps, 8.0\ ps$
Input probe power $P_{CW} = P_{probe}(0)$	$2.5\ dBm$
Differential delay in AMZI τ	$2.0\ ps$

In Ref. [2] the critical pulse width τ_{cr}, below which the ultra-fast dynamics starts to impact the gain, is expressed as $\tau_{cr} = \varepsilon/(a v_g)$. With the parameters in Table 1 and a group index of 3.6, we get $\tau_{cr} = 8.9\ ps$. Thus, for an input pulse width of 1.8 ps we expect significant impact from ultra-fast dynamics.

Figure 2 illustrates the setup used in experiments presented in the remaining part of this paper. For the cross-gain modulation (XGM) experiment presented later in this section, the filters in Fig. 2 were replaced by a 5 nm wide BPF with the peak transmission wavelength centered on the probe carrier. The control signal source consists of a mode-locked fiber ring laser (ML-FRL), emitting a 10.5 GHz train of 1.8 wide (FWHM) pulses at 1548 nm, and a two-stage passive fiber-interleaver, which creates a 42 GHz clock signal or a high speed digital data word consisting of 4 marks. For the investigation of nonlinear patterning effects in section 4, we generated the 105 Gb/s data word "1111000000", by properly adjusting the relative delays in the interleaver. The clock or data signal is launched into the SOA along with

#8897 - $15.00 USD Received 26 September 2005; revised 22 November 2005; accepted 19 December 2005
(C) 2006 OSA

a CW beam from a distributed feedback laser at 1558 nm. Both signals pass through polarization controllers consisting of a half-wave plate (H) between two quarter-wave plates (Q), to align the polarization of both signals to a principle axis of the SOA. At the SOA output the probe spectrum is monitored on an optical spectrum analyzer (OSA) before being sent to an AMZI filter or a detuned BPF. The AMZI filter is realized in the polarization domain, and details on the implementation can be found in e.g. Ref. [17]. After filtering, the probe signal is cross-correlated with the 10.5 GHz clock signal of 1.8 ps wide pulses from the ML-FRL.

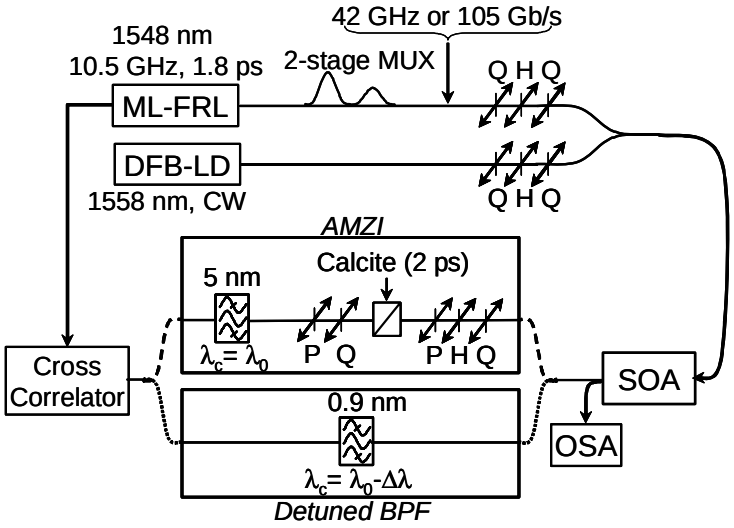

Fig. 2. Experimental setup

Figures 3 (a) and 3(b) shows a comparison between experimentally obtained cross correlation traces of cross-gain modulated probe signals at 1558 nm for data pulse widths of τ_p = 1.8 ps and 8 ps, respectively. The 8 ps wide pulses are obtained by propagating the 1.8 ps wide pulses through 215 m of standard single-mode fiber. In both cases the input is a periodic 105 Gb/s "1011010000" data signal with an energy of 133 fJ/pulse. In Fig. 3(a) two distinct time scales are observed during gain recovery: an ultra-fast recovery immediately after the control pulses, followed by the much slower inter-band carrier relaxation. In Fig. 3(b), where $\tau_p \approx \tau_{cr}$, the fast component is hardly visible. For comparison, traces simulated using the same input powers as in the experiment and the parameters in Table 1 are shown in Fig. 3(c) for $\tau_p = 1.8\,ps$ and in Fig. 3(d) for $\tau_p = 8\,ps$. The XGM traces are shown with (solid) and without (dashed) ultra-fast effects to emphasize that the excellent agreement with the experimental traces relies on the inclusion of nonlinear gain suppression. It should be noted that the scale is the same in all four plots.

#8897 - $15.00 USD Received 26 September 2005; revised 22 November 2005; accepted 19 December 2005
(C) 2006 OSA

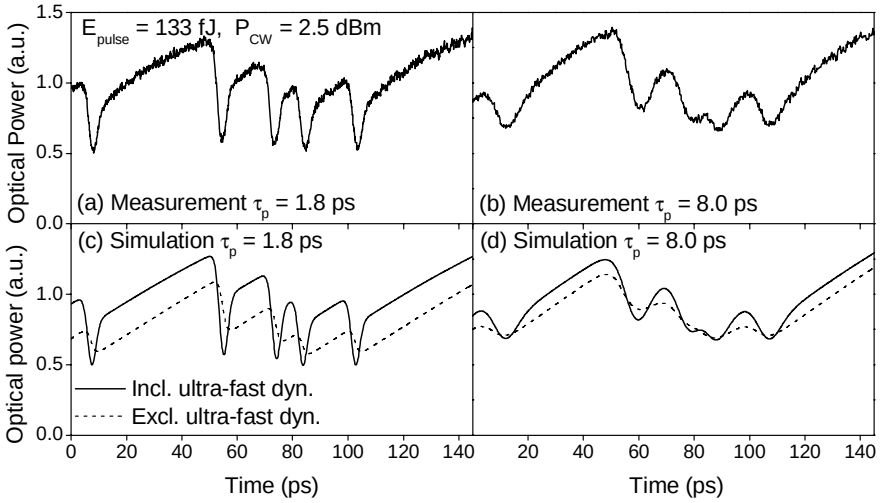

Fig. 3. Experimental 105 Gb/s XGM traces for (a) τ_p = 1.8 ps and (b) τ_p = 8.0 ps. Simulated traces incl. (solid) and excl. (dashed) ultra-fast dynamics for (c) τ_p = 1.8 and (d) τ_p = 8.0.

3. Spectral changes due to ultrafast dynamics

In this section the impact of ultra-fast dynamics on the optical power spectrum of the cross-gain and cross-phase modulated probe signal will be analyzed. Since the switches described in this paper consist of an SOA followed by optical filters it is important to understand how CH and SHB modify the relationship between the spectral components.

A previous theoretical analysis by Ueno et al., neglecting intra-band effects, provides an approximate, analytical expression for the spectral components $|E_n|^2 = |E(\omega = 2\pi n f_{rep})|^2$ of the probe power spectrum in the case where the control signal is a high frequency clock signal [16]

$$|E_n|^2 = \frac{4}{(2n\pi - \Delta\Phi_{lin})^2} \sin^2 \frac{2n\pi - \Delta\Phi_{lin}}{2} \qquad (10)$$

Here, $\Delta\Phi_{lin}$ is the carrier density induced phase shift provided by the clock signal of frequency nf_{rep}. This expression allows for estimating the induced phase shift by simply recording the probe spectrum. The phase shift $\Delta\Phi_{lin}$ is shown as a function of the ratio of the first blue component (n = 1) to the carrier peak (n = 0), $|E_1|^2 / |E_0|^2$, in the dashed curve in Fig. 4(a). From the results in Ref. [16] it is clear that the analytical approximation in Eq. (10) overestimates the obtainable phase shift slightly compared to a simulation. This is also observed in Fig. 4(a) by comparing the dashed curve to the black triangles, obtained with the model in section 2 for $\varepsilon_{SHB} = \varepsilon_{CH} = 0$ and a 42 GHz input clock signal consisting of 1.8 ps wide pulses. The circles in Fig. 4(a) correspond to including ultra-fast dynamics and in this case the approximation generally underestimates the phase shift. The reason for this is illustrated in Fig. 4(b), which shows two periods of the phase response including (excluding) ultra-fast effects in the solid (dashed) curve. The perfectly triangular response, shown in the short-dashed line, is the response assumed in the derivation of Eq. (10), and it is clear that the approximated magnitude of the phase shift $\Delta\Phi_{app}$ falls between the phase shifts $\Delta\Phi_{lin}$ and

#8897 - $15.00 USD Received 26 September 2005; revised 22 November 2005; accepted 19 December 2005
(C) 2006 OSA

$\Delta\Phi$ obtained by excluding and including ultra-fast effects, respectively, for an input pulse energy of 20 fJ. That is, $\Delta\Phi_{app}$ actually slightly overestimates the phase shift obtainable without ultra-fast effects. The conclusion from Fig. 4 is that including ultra-fast dynamics does not change the fact that the phase shift can be estimated from the ratio of the first blue-to-carrier ratio $|E_1|^2 / |E_0|^2$. However, it should be noted that the estimate is conservative. In Fig. 4(b) the phase shift $\Delta\Phi$ is divided into the phase shift $\Delta\Phi_N$ due to carrier density modulation and $\Delta\Phi_{CH}$ due to CH, in accordance with Eq. (5).

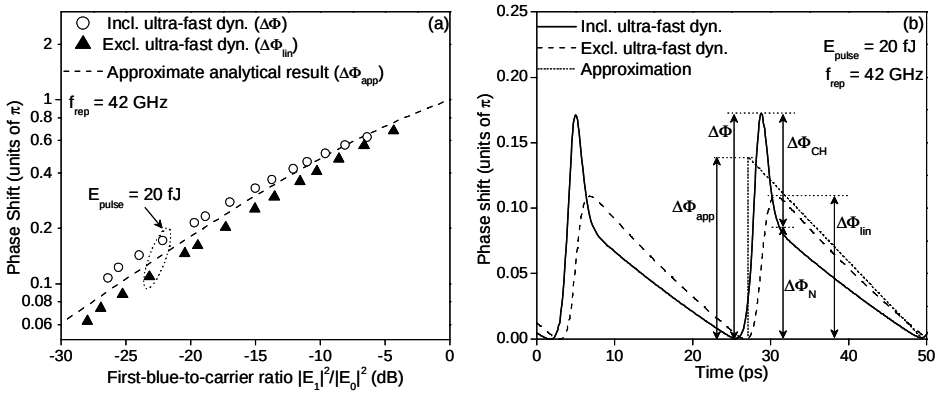

Fig. 4. (a) Calculated probe phase shift, induced by a 42 GHz pulse train, vs. the ratio $|E_1|^2 / |E_0|^2$ including ultra-fast dynamics, $\Delta\Phi$ (white circles), excluding ultra-fast dynamics, $\Delta\Phi_{lin}$ (black triangles), and the analytical result from Eq. (10). (b) Probe phase response vs. time, including (solid curve) and excluding (dashed) ultra-fast effects. Triangular response assumed in Eq. (10) shown in short-dashed line.

The impact of ultra-fast effects on the probe spectrum has been studied theoretically and the calculated spectra have been compared with experimental data to verify that the good agreement obtained in the time domain (see Fig. 3) is also mirrored in the frequency domain. Figure 5(a) shows a normalized experimental probe spectrum (solid curve) for a 42 GHz control signal input with a pulse energy of 133 fJ. Superimposed on the graph are the numerically calculated spectral components including (black triangles) and excluding (white squares) ultra-fast effects. It is observed that on the blue side of the carrier ($n > 0$), and for the three lowest harmonics on the red side, the model reproduces the experimental spectrum very well when ultra-fast effects are included. Without ultra-fast dynamics the deviation is large over the blue sideband as well as for the two lowest red harmonics. As observed in Fig. 4(b), CH causes a decrease of the phase following the excitation, which occurs on the time scale of the pulse width, and thus corresponds to a large spectral blue-shift. This is the reason for the larger spectral broadening observed of the blue sideband in Fig. 5(a). As discussed in Ref. [18], underestimation of the XPM-induced broadening of the blue side of the carrier seems to be a general problem even for advanced models including detailed treatments of amplified spontaneous emission, wavelength dependent gain, and waveguide loss. Figure 5(a) strongly suggests that the spectral discrepancy observed for those models is due to the neglect of ultra-fast gain and phase recovery.

In Fig. 5(b) the ratio of the first, third, and fifth blue 42 GHz harmonic to the carrier has been calculated with (solid) and without (dashed) ultra-fast dynamics, as a function of the pulse energy. The results are compared to the experimental values, and since the fast effects primarily impact the high-frequency components, it is expected that the solid and dashed

#8897 - $15.00 USD Received 26 September 2005; revised 22 November 2005; accepted 19 December 2005
(C) 2006 OSA

curved deviate more for higher harmonics. As observed, the agreement between the experimental data and the simulations is only good when ultra-fast effects are included.

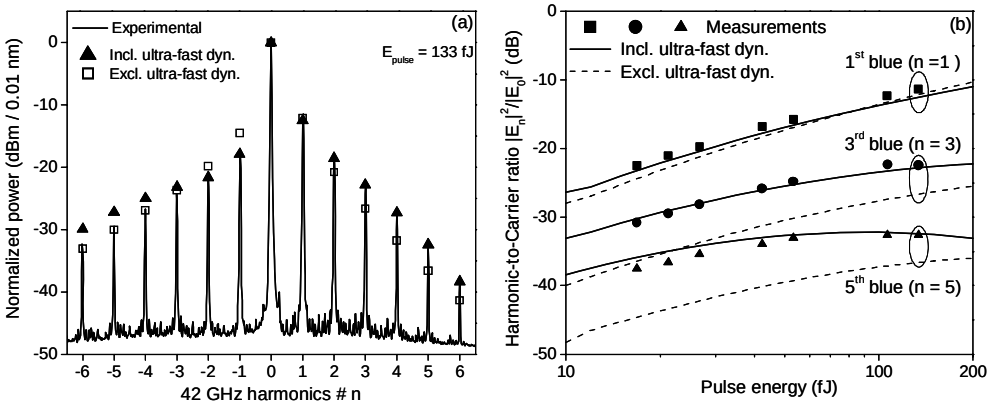

Fig. 5. (a) Comparison of normalized probe power spectra for 42 GHz input pulse train: Experimental (solid curve), simulations including (black triangles) and excluding (white squares) ultra-fast effects. (b) Ratio power in first, third, and fifth blue 42 GHz harmonic to the power in the carrier peak vs. input pulse energy. Experimental (black symbols), simulations including (solid curves) and excluding (dashed curves) ultra-fast effects.

4. Impact of ultrafast dynamics on nonlinear pattering

The amount of nonlinear patterning (NLP) observed at the output of a DISC switch, and other SOA+filter-based switches, depends on the variation of the probe phase shift induced by the data signal [8]. The more saturated the SOA becomes, i.e. the more consecutive pulses with high energy are launched into the SOA, the larger the variation of the induced phase shift becomes, and consequently a larger variation of the switched pulse energy is observed.

With the experimental setup in Fig. 2, periodic word patterns with a maximum of four marks (four pulses) per word can be created. This sets an upper limit to the amount of NLP that will be observed for a given pulse energy. To maximize the NLP, i.e. to obtain the worst-case scenario with the available four pulses, we generated the 105 Gb/s pattern "1111000000", which creates the largest carrier density variation. For comparison we use the same pattern in the simulations, and an example is shown in Fig. 6 for 1.8 ps pulses with energy of 20 fJ, showing (a) the gain, (b) the phase, (c) the DISC output power, and (d) DISC output power normalized to the peak power of the first pulse. Moreover, Fig. 6(c) shows how NLP is quantified, namely as the *ratio* of the largest to the smallest switched peak pulse power. The calculation is done both with (solid) and without (dashed) ultra-fast effects, and in contrast to the previous calculations, the waveforms have *not* been convoluted with the 1.8 ps wide sech^2 pulse, because this conceals important details. Focusing first on the DISC output in Fig. 6(c) and (d), which are realized with the AMZI parameters $(\tau, \Phi_0) = (2\,ps, 0.988\pi)$, three things are observed: the CH-induced "overshoot" $\Delta\Phi_{CH}$ in the phase response causes a larger differential phase shift $\Phi(t) - \Phi(t-\tau)$, which results in an increased switched output pulse energy and thus a larger optical signal-to-noise ratio (OSNR), compared to the case without ultra-fast effects. In addition, the phase "overshoot" creates a trailing satellite pulse after each switched pulse. This phenomenon was also reported in Ref. [3], and even without ultra-fast effects it is found in Ref. [19] that satellite pulses can be generated under certain conditions. The satellite pulses may present a problem during transmission because they are chirped differently from the main pulse. However, an investigation of this effect is considered outside the scope of this work.

#8897 - $15.00 USD Received 26 September 2005; revised 22 November 2005; accepted 19 December 2005
(C) 2006 OSA

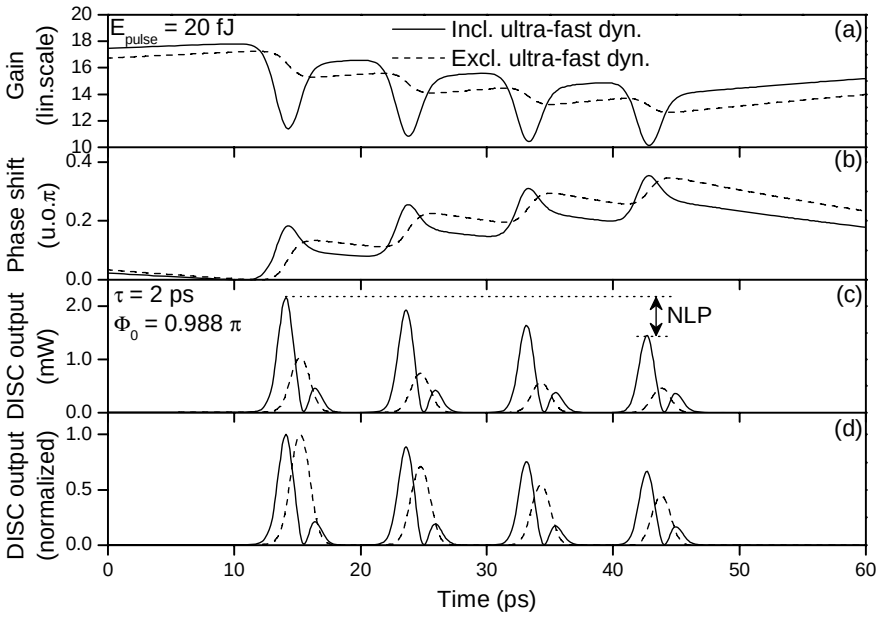

Fig. 6. Simulation of (a) SOA gain and (b) probe phase for input control signal "1111000000" with pulse energy of 20 fJ. (c) Corresponding DISC output incl. definition of NLP, and (d) normalized DISC output for AMZI parameters $(\tau, \Phi_0) = (2\,ps, 0.988\pi)$. Solid curves (dashed curves) correspond to inclusion (exclusion) of ultra-fast effects

Finally, from the normalized plot in Fig. 6(d) it is clear that ultra-fast dynamics reduces NLP, which is formally defined in Fig. 6(c) for the present pattern. The reason for this is the nonlinear gain suppression, i.e. the additional gain saturation caused by the ultra-fast effects, which reduces the carrier density depletion by reducing the control pulse energy and thus the stimulated recombination rate [3,4]. The reduced carrier density dependent contribution to the phase shift, $\Delta\Phi_N(t)$, is clearly visible in Fig. 6(b). The fact that the amount of carriers depleted per data pulse is diminished prompts a reduction of the carrier density dependent contribution to NLP [8]. As explained above, the reduced $\Delta\Phi_N(t)$ is more than made up for by the "overshoot" induced by $\Delta\Phi_{CH}(t)$. However, it is clear from Eq. (5) that the patterning of $\Phi_{CH}(t)$ is determined by the patterning of the gain $G(t)-1=\exp\left[g_m(t)\right]-1$, which is reduced by nonlinear gain suppression, as illustrated in Fig. 6(a). In conclusion, ultra-fast dynamics increases the phase modulation while reducing the carrier depletion, which is a desirable combination of events, as it increases the OSNR while reducing NLP. The effect of the reduced rate of carrier depletion is that it takes a longer sequence of consecutive pulses to induce a certain amount of NLP. It is important to note that for a constant average power of the switched signal, the required input data pulse energy will be *smaller* in the presence of ultra-fast effects, thus making the NLP reduction even more pronounced.

Figure 7 shows a comparison of switched probe waveforms at the output of the DISC for the input pattern "1111000000" with pulse energies of 17, 53, and 133 fJ. The traces are obtained (a) numerically, excluding ultra-fast effects, (b) including ultra-fast effects, and (c) experimentally. In all cases the power is normalized to the peak power of the first pulse in the four-pulse sequence, and the simulated traces are convoluted with the 1.8 ps sech^2 pulse to simulate cross-correlation. As expected, the NLP predicted by the simulations is significantly

#8897 - $15.00 USD Received 26 September 2005; revised 22 November 2005; accepted 19 December 2005
(C) 2006 OSA

reduced by including ultra-fast dynamics, but the model still overestimates the experimentally observed patterning.

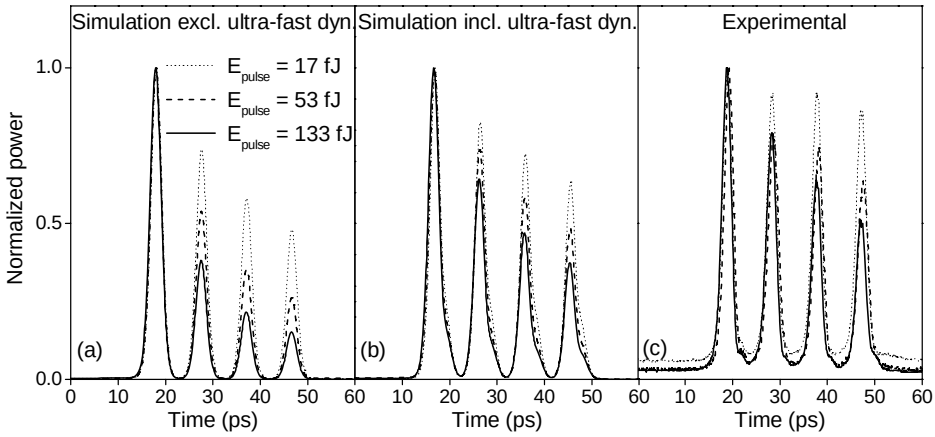

Fig. 7. Normalized switched output for input control signal "1111000000" with pulse energy of 17 fJ (dotted), 53 fJ (dashed), and 133 fJ (solid). Simulation (a) excluding and (b) including ultra-fast dynamics, compared to the experimental results in (c).

Notice that the satellite pulse observed in Fig. 6(c),and 6(d) turns into a trailing pedestal after the convolution in Fig. 7(b). By careful inspection of Fig. 7(c) a slight pedestal is actually also observed experimentally, particularly for $E_{pulse} = 133\text{fJ}$ and after the last pulse.

A quantitative comparison of the modeled and experimental NLP is given in Fig. 8. The overestimation of NLP by the model suggests that there may be additional contributions to the gain suppression factor ε that have not been accounted for, or alternatively that the α_{CH} -parameter is larger than assumed in Table 1, since both will tend to reduce the NLP. In Fig. 8 the dotted curve corresponds to an unrealistically high gain suppression factor for CH, $\varepsilon_{CH} = 7.5 \cdot 10^{-23} m^3$, which is observed to fit the experimental points very well. However, with this value the spectral properties presented in section 3 are not verified, and as mentioned, the value is far beyond the limits of what has been observed experimentally.

#8897 - $15.00 USD Received 26 September 2005; revised 22 November 2005; accepted 19 December 2005
(C) 2006 OSA

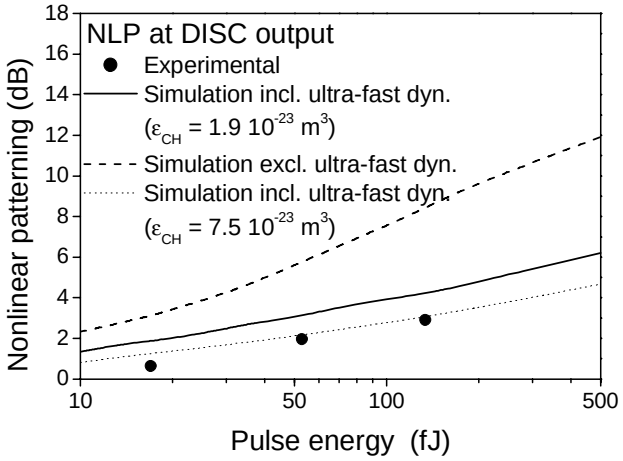

Fig. 8. Nonlinear patterning at DISC output vs. input pulse energy. Experimental (black dots), simulation including (solid) and excluding (dashed) ultra-fast effects. Simulation for unrealistically large $\varepsilon_{CH} = 7.5 \cdot 10^{-23} m^3$ is shown in dotted curve.

As detailed in [8] the AMZI is just one example of a filter that is able to equalize the linear patterning effects caused by the relatively slow carrier recovery. Band-pass filters detuned to one of the sidebands of the probe spectrum provide similar bandwidth enhancing properties, and in addition it has been shown experimentally, currently at bitrates up to 80 Gb/s, that a low NLP can be obtained as well [12,13].

To investigate the impact of ultra-fast effects on a switch consisting of an SOA and a BPF, the AMZI is replaced by a 0.9 nm wide (FWHM) BPF, with a frequency response that can be modeled as a Gaussian shape with reasonable accuracy. The modeling is carried out both excluding and including ultra-fast effects, as shown in Fig. 9(a)-9(d) and Fig. 9(e)-9(h), respectively, for four different filter detunings from the carrier of 0, -0.7 nm, -1.3 nm, and -1.5 nm. The calculations are compared to the experimental results in Fig. 9(i)-9(l). The pulse energy is as high as 133 fJ, which gave the best experimental results. From the comparison in Fig. 9, it is clear that ultra-fast dynamics also reduces NLP for this switch configuration. Moreover, the waveforms computed by including ultra-fast effects are in much better agreement with the experimental traces, which once again underlines the importance of including these effects. Notice that for small negative (blue) wavelength detuning of the BPF the signal polarity remains inverted [see Fig. 9(b), 9(f), and 9(j)], but the recovery rise-time is reduced. This is due to the relative enhancement of the blue-shifted rising edge compared to the red-shifted falling edge, and may be referred to as filtering-assisted XGM, which has been demonstrated in systems-type experiments up to 100 Gb/s, with a large power penalty though Ref. [23]. When the BPF is detuned further to the blue side the power in the carrier peak, which determines the mark-level of the inverted signal, is suppressed to a point where the polarity changes from inverted back to non-inverted [see Fig. 9(c), 9(g),and 9(k)]. In this scenario, XPM is the dominant process, since the filter transmission peak is positioned on the sideband, which exists primarily due to XPM. For BPF detunings between -0.7 nm and -1.3 nm the waveform undergoes polarity change and will thus be distorted. This is illustrated in Ref. [12]. The nonlinear patterning observed in Fig. 9(c), 9(g),and 9(k) for $\Delta\lambda = -1.3nm$ can be reduced by detuning the filter further, as illustrated in Fig. 9(d), 9(h),and 9(l). This is the case because, at the output of the filter, the leading pulses are less blue-shifted than the trailing pulses.

#8897 - $15.00 USD Received 26 September 2005; revised 22 November 2005; accepted 19 December 2005
(C) 2006 OSA

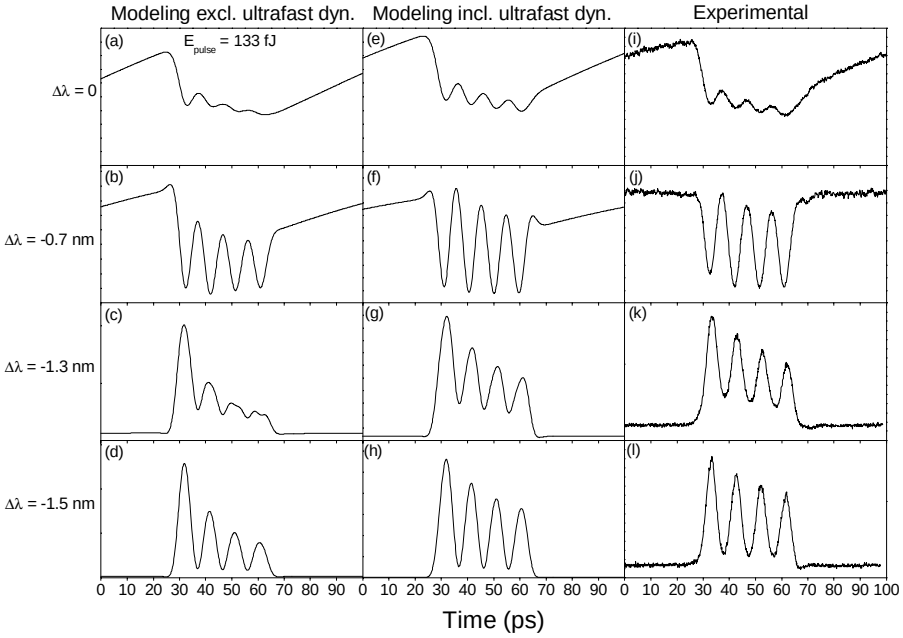

Fig. 9. Switched waveforms for SOA + detuned 0.9 nm wide BPF, using input control signal "1111000000" with pulse energy of 133 fJ. Filter detuning is 0, -0.7 nm, -1.3 nm, and -1.5 nm from top row to bottom row. First (second) column shows simulated waveforms excluding (including) ultra-fast effects, and third column shows corresponding experimental results.

The reduced NLP obtained by detuning the filter comes at the price of reduced output power, which introduces a clear trade-off between low patterning and high OSNR. This is illustrated in Fig. 10(a), which shows the calculated NLP (left axis) and calculated transmitted average power (right axis) for a pulse energy of 133 fJ, as a function of the detuning of the 0.9 nm wide Gaussian BPF. As explained above the polarity is inverted for moderate blue and red detunings, and preserved beyond the limits indicated by the dotted, vertical lines. The results are shown both including (solid) and excluding (dashed) ultra-fast dynamics, and a significant difference is observed for the degree of patterning effects. The black dots indicate the experimentally observed NLP from Fig. 9(k) and 9(l), which are again below the calculated curve. Two important details should be noticed in Fig. 10(a): the first is that the NLP is significantly smaller for negative (blue) filter detunings, compared to positive (red) detunings. The reason for this, as detailed in Ref. [18], is that the patterning of the blue chirp is significantly smaller than that of the red chirp. This is so because the blue shift stems from the *recovery* of the phase response, which occurs right *after* gain saturation, whereas the red chirp stems from stimulated recombination, which takes place during depletion. Thus, the carrier density variation, and by that the NLP experienced by the blue-shifted spectral components, is smaller than that of the red-shifted counterparts. It should be noted that the variation in NLP between the blue and red sidebands increases with pulse energy, which means that good results may be obtained by filtering on the red sideband by reducing the control pulse energy. The second important detail in Fig. 10(a) is that the ultra-fast effects, in addition to reducing NLP, also further broadens the probe spectrum, which increases the power, and thus the OSNR, of the signal transmitted from the filter.

It is important to stress that *without* including ultra-fast carrier dynamics the NLP effect can only be reduced by lowering the carrier recovery time through the use of a holding beam. However, this recovery time is readily available through simple experiments, and to obtain the same level of NLP in a model *without* ultra-fast dynamics as can be obtained *with* ultra-fast dynamics, the carrier recovery time would have to be reduced to an unrealistically low level.

#8897 - $15.00 USD Received 26 September 2005; revised 22 November 2005; accepted 19 December 2005
(C) 2006 OSA

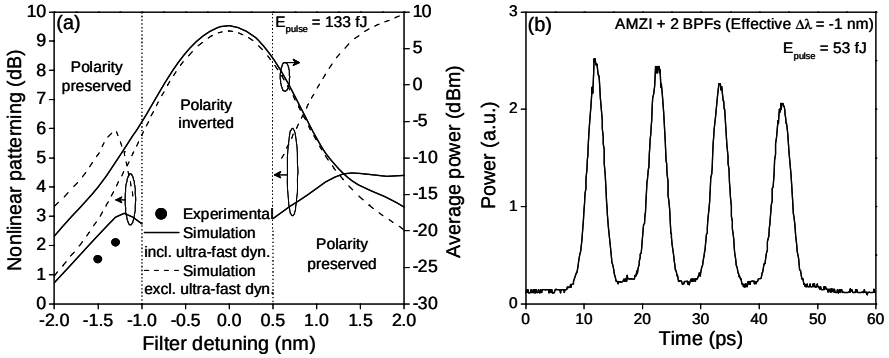

Fig. 10. (a) Simulated nonlinear patterning (left axis) and switched average power (right axis) vs. detuning of 0.9 nm wide BPF after SOA, for input control signal "1111000000" with pulse energy of 133 fJ. Solid (dashed) curves correspond to including (excluding) ultra-fast effects. Black dots indicate experimental nonlinear patterning. (b) Waveform at the output of AMZI + 2 BPF cascade. The effective FWHM bandwidth and detuning of the 2 BPFs are 2.4 nm and -1.0 nm, respectively.

From the results presented above, it seems logical to investigate the impact of cascading the AMZI with a detuned BPF. In a theoretical study of "pulse reformatting filters" [20], which ideally eliminate all patterning effects, the optimum filter power transfer function was found to resemble a cascade of a an AMZI and a BPF. An approximation to this filter was realized and produced excellent results at 40 Gb/s. Moreover, the AMZI+BPF cascade was recently used to successfully demonstrate 160 Gb/s wavelength conversion [11], which illustrates the potential of this configuration. A basic theoretical (excl. ultra-fast dynamics) and experimental investigation of the dependence of NLP on BPF detuning was carried out in Ref. [15] for a periodic 43 Gb/s "1100" pattern. It was demonstrated that NLP is clearly reduced by blue-detuning the BPF, again at the expense of the output power and OSNR. Here, the pattern in Fig. 10(b) shows the result of cascading the AMZI with two BPFs, with bandwidths of 2.7 nm and 5 nm, for a pulse energy of 53 fJ. The BPFs are detuned by different amounts, so that the total transfer function has a bandwidth of 2.4 nm, different slopes on the two edges of the pass-band, and a transmission maximum $\Delta\lambda = -1.0nm$ away from the carrier. This reduces the NLP from the 1.96 dB observed in Fig. 8 to 0.87 dB in Fig. 10(b).

Compared to other fast all-optical switch configurations, such as e.g. the SOA-MZI operated in differential (push-pull) mode [16,17], the concept of a single SOA followed by a, potentially integratable, optical filter is very simple and attractive. The choice of filter should be based on the following four parameters: i) magnitude of NLP for specific output power, ii) OSNR, iii) fabrication cost, and iv) mechanical and thermal stability. From the experiments and simulations presented in this paper and in Refs. [11-13] it is clear that there is a serious trade-off between low NLP and high OSNR. That speaks in favor of realizing the appropriate filter transfer function as a cascade of individual filters, e.g. an AMZI+BPF cascade, since this allows for amplification in-between the filters. In practice the switch is likely to be followed by a booster amplifier, as illustrated in Fig. 1, and amplification in-between the two filters will help keep the switch output power at a sufficiently high level to saturate the booster amplifier, thereby adding less ASE to the signal, and improving the OSNR. Another advantage of the AMZI filter is that it suppresses ASE inside the signal bandwidth, which provides an addition OSNR improvement [17]. A linear quantum dot (QD) SOA with high output saturation power and low noise figure would be a good choice for an intermediate amplifier, due to its superior performance and compactness [24]. For co-propagating data and probe signals, a BPF at the output is required to suppress the data signal, even if an AMZI is chosen as the pulse shaping filter. Thus, cascading the AMZI and the detuned BPF does not require additional components

#8897 - $15.00 USD Received 26 September 2005; revised 22 November 2005; accepted 19 December 2005
(C) 2006 OSA

compared to the standard DISC configuration, except for the optional QD-SOA if the detuned BPF attenuates the signal prohibitively. The cascade may produce favorable results for parameter i, ii, and iv above, but obviously an intermediate amplifier will add significantly to the cost, unless the nonlinear SOA, the AMZI, and the linear SOA can be integrated.

5. Summary

In summary, we have investigated the impact of ultra-fast carrier dynamics due to spectral hole-burning (SHB) and carrier heating (CH) on the performance of high-speed all-optical switches, based on a single SOA and an optical filter. Through modeling and comparison with experiments the fast effects are identified as the reason for an experimentally observed large spectral broadening on the blue side of probe carrier wavelength, which by itself enhances the power transmitted by the switches, and ultimately the optical signal-to-noise ratio (OSNR). A previously published analytical relationship between the induced phase shift and the suppression of the first blue harmonic in the probe spectrum, derived without attention to ultra-fast effects, was found to be equally accurate when fast dynamics is included. The nonlinear patterning effects, which manifest as peak pulse power fluctuations of the switched signal, were analyzed and quantified through simulations and experiments at 105 Gb/s on three different switches consisting of an SOA and an asymmetric MZI (AMZI) filter, a detuned band-pass filter (BPF), and a cascade of an AMZI and a detuned BPF. Ultra-fast nonlinearities are found to dramatically reduce the nonlinear patterning, while improving the OSNR. This leads us to the conclusion that fast dynamics has played an important role in the success of the high-speed demonstrations (> 100 Gb/s) reported in the literature. Moreover, we show that a blue detuning of the BPF peak transmission wavelength reduces the nonlinear patterning, regardless of whether the BPF is positioned right after the SOA or after the SOA *and* an AMZI filter. The detuning is shown to introduce a clear trade-off between patterning reduction and OSNR.

Of the three filters analyzed, we identify the cascade of the AMZI and detuned BPF as the best choice. The output power from the AMZI is still sufficiently high that the signal can be amplified without a notably power penalty, allowing to compensate for the attenuation suffered in the following BPF.

#8897 - $15.00 USD Received 26 September 2005; revised 22 November 2005; accepted 19 December 2005
(C) 2006 OSA